Coupled magnetic and structural phase transitions in the antiferromagnetic polar metal Pb_2CoOsO_6 under pressure

Yuanyuan Jiao,[1,2,*,†] Yue-Wen Fang,[3,4,*] Jianping Sun,[1,2] Pengfei Shan,[1,2] Zhenhai Yu,[5] Hai L. Feng,[1] Bosen Wang,[1,2,6] Hanming Ma,[7] Yoshiya Uwatoko,[7] Kazunari Yamaura,[8,9] Yanfeng Guo,[5,‡] Hanghui Chen,[4,10,§] and Jinguang Cheng[1,2,6,‖]

[1]*Beijing National Laboratory for Condensed Matter Physics, Institute of Physics, Chinese Academy of Sciences, Beijing 100190, China*
[2]*School of Physical Sciences, University of Chinese Academy of Sciences, Beijing 100190, China*
[3]*Laboratory for Materials and Structures & Tokyo Tech World Research Hub Initiative (WRHI), Institute of Innovative Research, Tokyo Institute of Technology, 4259 Nagatsuta, Midori-ku, Yokohama, Kanagawa 226-8503, Japan*
[4]*NYU-ECNU Institute of Physics, New York University Shanghai, Shanghai, 200062, China*
[5]*School of Physical Science and Technology, ShanghaiTech University, Shanghai 201210, China*
[6]*Songshan Lake Materials Laboratory, Dongguan, Guangdong 523808, China*
[7]*Institute for Solid State Physics, University of Tokyo, Kashiwa, Chiba 277-8581, Japan*
[8]*International Center for Materials Nanoarchitectonics (WPI-MANA), National Institute for Materials Science, Tsukuba 305-0044, Japan*
[9]*Graduate School of Chemical Science and Engineering, Hokkaido University, Sapporo 060-0810, Japan*
[10]*Department of Physics, New York University, New York 10012, USA*

(Received 20 July 2020; accepted 21 September 2020; published 13 October 2020)

Pb_2CoOsO_6 is a newly synthesized polar metal in which inversion symmetry is broken by the magnetic frustration in an antiferromagnetic ordering of Co and Os sublattices. The coupled magnetic and structural transition occurs at 45 K at ambient pressure. Here, we perform transport measurements and first-principles calculations to study the pressure effects on the magnetic/structural coupled transition of Pb_2CoOsO_6. Experimentally, we monitor the resistivity anomaly at T_N under various pressures up to 11 GPa in a cubic anvil cell apparatus. We find that T_N determined from the resistivity anomaly first increases quickly with pressure in a large slope of $dT_N/dP = +6.8(8)$ K/GPa for $P < 4$ GPa and, then, increases with a much reduced slope of 1.8(4) K/GPa above 4 GPa. Our first-principles calculations suggest that the observed discontinuity of dT_N/dP around 4 GPa may be attributed to the vanishing of the Os magnetic moment under pressure. Pressure substantially reduces the Os moment and completely suppresses it above a critical value, which relieves the magnetic frustration in the antiferromagnetic ordering of Pb_2CoOsO_6. The Co and Os polar distortions decrease with the increasing pressure and simultaneously vanish at the critical pressure. Therefore, above the critical pressure, a new centrosymmetric antiferromagnetic state emerges in Pb_2CoOsO_6, distinct from the one under ambient pressure, thus, showing a discontinuity in dT_N/dP.

DOI: 10.1103/PhysRevB.102.144418

I. INTRODUCTION

Ferroelectricity is usually incompatible with long-range magnetic order and metallicity [1–3]. Insulating materials which possess both electric polarization and magnetization and possibly a coupling between the two order parameters are called multiferroics, which has been an active research field in condensed-matter physics and materials science [4–6]. On the other hand, materials with both polar displacements and intrinsic metallicity are termed "polar metals" [3,7], which have attracted increasing interest in experiment and theory [8–17]. Accordering to Anderson and Blount [3], polar metals are characterized by a second-order structural phase transition with the appearance of a polar axis and the loss of inversion symmetry at a finite temperature. $LiOsO_3$ is the first unambiguous example of bulk polar metals, which transforms from a centrosymmetric $R\bar{3}c$ structure to a polar $R3c$ structure at $T_s = 140$ K [7,18]. However, a *metal* that possesses both polar displacements and magnetization and most importantly a coupling between the two is extremely rare. Previous theoretical proposals of cation-ordered $SrCaRu_2O_6$ [9] and $BiPbTi_2O_6$ [17] show the coexistence of ferromagnetism with polar displacements but there is no strong coupling between the two properties.

Recently, Princep and coworkers have synthesized a new polar metal Pb_2CoOsO_6 in which an antiferromagnetic order with magnetic frustration breaks the inversion symmetry [19]. Pb_2CoOsO_6 crystallizes in a cation-ordered double-perovskite structure. At room temperature, the material is paramagnetic and centrosymmetric with space-group $P2_1/n$ (No. 14). At $T = 45$ K, Pb_2CoOsO_6 undergoes a continuous phase transition to an antiferromagnetically ordered state

*These two authors contributed equally to this work.
†Present address: Faculty of Science, Wuhan University of Science and Technology, Wuhan, Hubei 430065, China.
‡guoyf@shanghaitech.edu.cn
§hanghui.chen@nyu.edu
‖jgcheng@iphy.ac.cn

with propagation vector $\mathbf{k} = (1/2, 0, 1/2)$. Both Co and Os atoms have magnetic moments and they order simultaneously. Accompanying the appearance of magnetic order is the removal of inversion symmetry. This is because each Os moment is surrounded by six neighboring Co moments, three of which are parallel to the Os moment and the other three of which are antiparallel to the Os moment. The ferromagnetic and antiferromagnetic couplings between Os and Co moments are generically different and, thus, this magnetic frustration forces the Os moment to move away from the centrosymmetric position, which breaks the inversion symmetry. The low-temperature polar structure has space-group P_c (No. 7) with the corresponding Shubnikov group for the magnetic structure being P_ac. Since in Pb_2CoOsO_6, the polar displacements are induced by the unique long-range magnetic order, similar to "type-II multiferroics" [20], we may term Pb_2CoOsO_6 as "type-II polar metals," whereas $SrCaRu_2O_6$ [9] and $BiPbTi_2O_6$ [17] may be referred to as "type-I polar metals" since magnetic order and polar displacements have different sources and are weakly coupled in these materials.

In comparison with ferroelectrics, polar metals usually exhibit a much lower structural transition temperature, e.g., $T_s =$ 140 K for $LiOsO_3$ [7] and $T_s(= T_N) = 45$ K for Pb_2CoOsO_6 whereas the T_s for a prototypical ferroelectric material $BaTiO_3$ is above room temperature. From the viewpoint of the practical applications, it is desirable to increase the transition temperature of polar metals. By monitoring the resistivity anomaly at T_s of $LiOsO_3$ under different pressures up to 6.5 GPa, Aulestia and coworkers have reported that the application of hydrostatic pressure can significantly enhance its nonpolar to polar transition temperature with a linear slope of $dT_s/dP \approx 17.54$ K/GPa, reaching approximately 250 K at 6.5 GPa [18]. Based on the first-principles calculations, the enhancement of T_s in $LiOsO_3$ has been attributed to the fact that pressure stabilizes the polar metallic state with a smaller unit-cell volume than the nonpolar state. The pressure effect of increasing T_s in $LiOsO_3$ is different from that in $BaTiO_3$ in which pressure reduces its T_s [21,22].

In this paper, we study the pressure effect on the newly synthesized type-II polar metal Pb_2CoOsO_6 by monitoring the resistivity anomaly at T_N under various pressures up to 11 GPa in a cubic anvil cell (CAC) apparatus. We find that similar to $LiOsO_3$, the transition temperature $T_s = T_N$ is also increased by pressure. But interestingly, T_N as a function of pressure P increases with pressure with a discontinuous change in slope from $dT_N/dP = 6.8(8)$ K/GPa for $P < 4$ GPa to 1.8(4) K/GPa for $P > 4$ GPa. Our first-principles calculations suggest that the change in dT_N/dP can be attributed to the vanishing of the Os magnetic moment. Under pressure, the Os moment is reduced and completely suppressed above a critical value. Above the critical pressure, the magnetic frustration is relieved, and the inversion symmetry is restored, which leads to a distinct magnetic metallic state.

II. EXPERIMENTAL AND COMPUTATIONAL DETAILS

Pb_2CoOsO_6 single crystals were grown under high-pressure and high-temperature conditions as described elsewhere [19]. Temperature dependences of magnetic susceptibility and resistivity at ambient pressure were measured

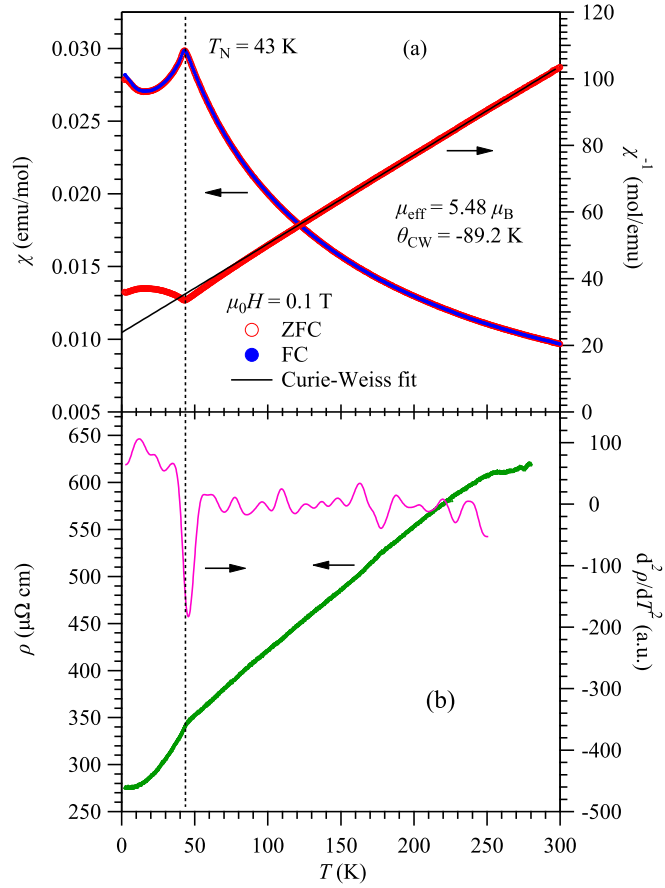

FIG. 1. Temperature dependences of (a) magnetic susceptibility $\chi(T)$ and its inverse $\chi^{-1}(T)$, and (b) resistivity $\rho(T)$ and its derivative $d\rho/dT$ for the Pb_2CoOsO_6 single crystal. The antiferromagnetic transition at $T_N = 43$ K is marked by a vertical broken line.

on the Magnetic Properties Measurement System and Physical Property Measurement System from Quantum Design, respectively. We have carried out high-pressure resistivity measurements on Pb_2CoOsO_6 single crystals with the standard four-probe method by using a palm CAC apparatus. Glycerol was employed as the pressure transmitting medium, and the pressure values were determined from the pressure-loading force calibration curve at room temperature. Glycerol may produce some nonhydrostatic stress [23,24], but it is not expected to affect the reported results. Details about the experimental setup can be found elsewhere [25].

We perform spin-polarized density functional theory (DFT) calculations using a plane-wave basis set and projector-augmented-wave method [26] as implemented in the Vienna *Ab initio* Simulation Package (VASP) [27,28]. We take into account spin-orbit coupling (SOC) in the DFT calculations and test the Hubbard U effect. We use PBEsol [29]—a revised Perdew-Burke-Ernzerhof (PBE) generalized gradient approximation for improving equilibrium properties of densely packed solids as the exchange-correlation functional. We start from the experimental crystal structure [19] and perform structural optimization under the studied pressures until each Hellmann-Feynman force component is smaller than 10^{-3} eV Å^{-1}. We use the magnetic ordering obtained from

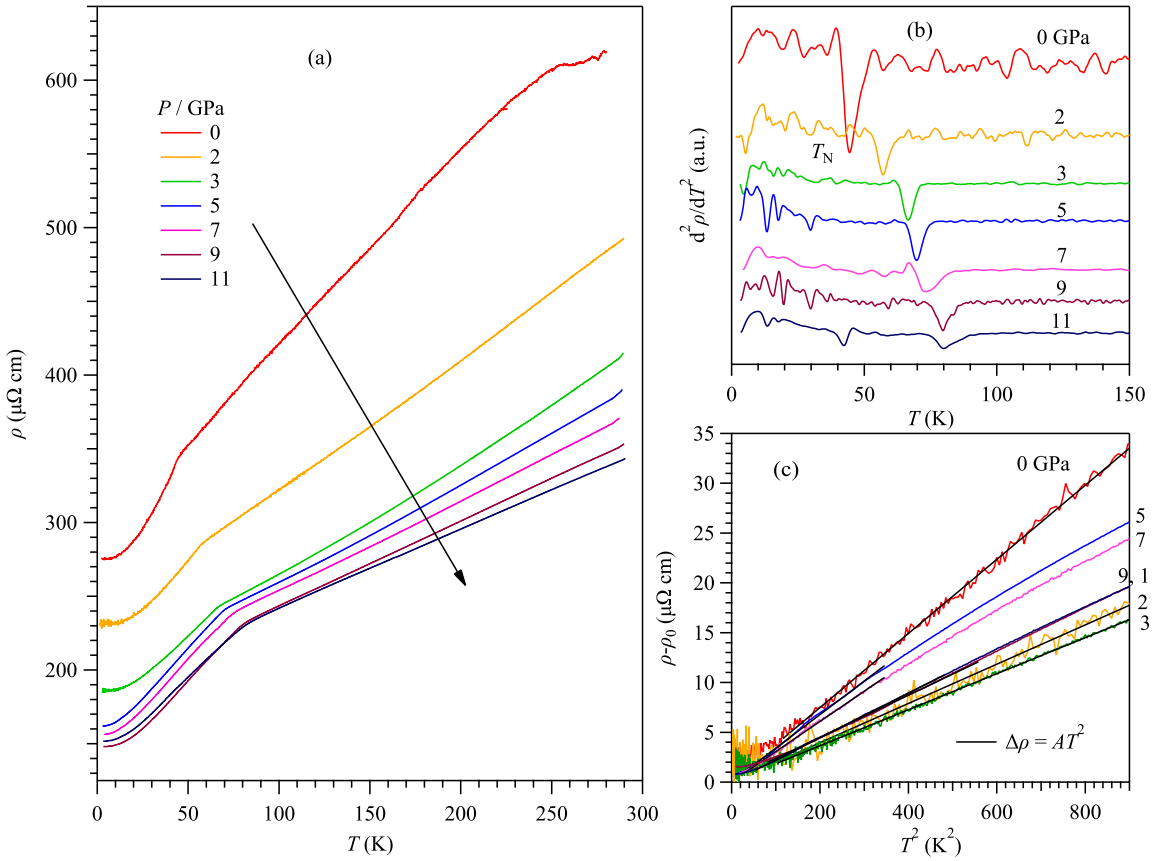

FIG. 2. Temperature dependences of (a) resistivity $\rho(T)$ and (b) its second derivative $d^2\rho/dT^2$ under various pressures up to 11 GPa for the Pb_2CoOsO_6 single crystal. (c) A plot of $\delta\rho \equiv (\rho - \rho_0)$ versus T^2 for the $\rho(T)$ data at low temperatures. The solid lines are linear fitting curves to extract the quadratic-T coefficient A.

experimental neutron powder diffraction [19] in all our calculations, hence, a very large cell with 80 atoms is used for the calculation. The Brillouin-zone integration is performed with a Gaussian smearing of 0.05 eV over a Γ-centered $\boldsymbol{k}$ mesh of $6 \times 12 \times 6$. An energy cutoff of 600 eV is used in all the calculations. The threshold of energy convergence is 10^{-7} eV. We use a higher-energy cutoff (700 eV) and a denser $\boldsymbol{k}$ mesh ($8 \times 14 \times 8$), and we do not find any significant changes in the key results. Our test calculations including Hubbard U on Co and Os d orbitals in the approach of Dudarev *et al.* [30] find that electron correlation increases the magnetic moment on Co and Os. The DFT + U calculations ($U_{Co} = U_{Os} = 2$ eV) find that the magnetic moments of Co and Os are 2.75 and $1.53\mu_B$, respectively. In particular, the magnetic moment of Os is about 3.6 times the DFT-calculated Os moment of $0.43\mu_B$, which strongly deviates from the experimental value (experimentally Os moment $< 0.5\mu_B$). Hence, all the computational results presented in this paper are calculated by spin-polarized DFT calculations without Hubbard U.

III. RESULTS AND DISCUSSION

The studied Pb_2CoOsO_6 single crystal was first characterized at ambient pressure by measuring the magnetic susceptibility $\chi(T)$ and resistivity $\rho(T)$. The results are consistent with those published in previous report [19]. As shown in Fig. 1, zero-field-cooled and field-cooled $\chi(T)$ curves measured under $\mu_0 H = 0.1$ T are almost overlapped with each other and both exhibit a clear cusp anomaly at the long-range antiferromagnetic order at $T_N = 43$ K. A Curie-Weiss fitting to $\chi^{-1}(T)$ in the paramagnetic region above 150 K yields an effective magnetic moment of $\mu_{eff} = 5.48\mu_B$ per formula unit and a Curie-Weiss temperature of $\theta_{CW} = -89.2$ K, respectively. The obtained μ_{eff} is larger than the expected spin-only value of $4.8\mu_B$ by assuming high-spin Co(II) with $S = 3/2$ and Os(VI) with $S = 1$. This should be attributed to the fact that high-spin Co(II) in related double perovskites always have an effective moment higher than the spin-only value of $3.87\mu_B$ due to the presence of the unquenched orbital moment [31]. The negative θ_{CW} signals the presence of dominant net antiferromagnetic interactions that produce a moderate magnetic frustration, i.e., $|\theta_{CW}/T_N| \approx 2$ in this double perovskite. Pb_2CoOsO_6 is confirmed to be metallic in the whole temperature range, and its $\rho(T)$ displays a clear inflection point at T_N, which can be defined clearly from the minimum of $d^2\rho/dT^2$ as shown in Fig. 1(b). According to Ref. [19], the antiferromagnetic ordering involving both Co and Os sublattices will remove the inversion symmetry due to magnetic frustration and relax the structure into a polar structure (P_c). Therefore, we can track the pressure dependence of the coupled antiferromagnetic/structural transition by monitoring the resistivity anomaly at T_N under high pressures.

Figure 2(a) displays the $\rho(T)$ curves of Pb_2CoOsO_6 under various pressures up to 11 GPa. As can be seen, it remains

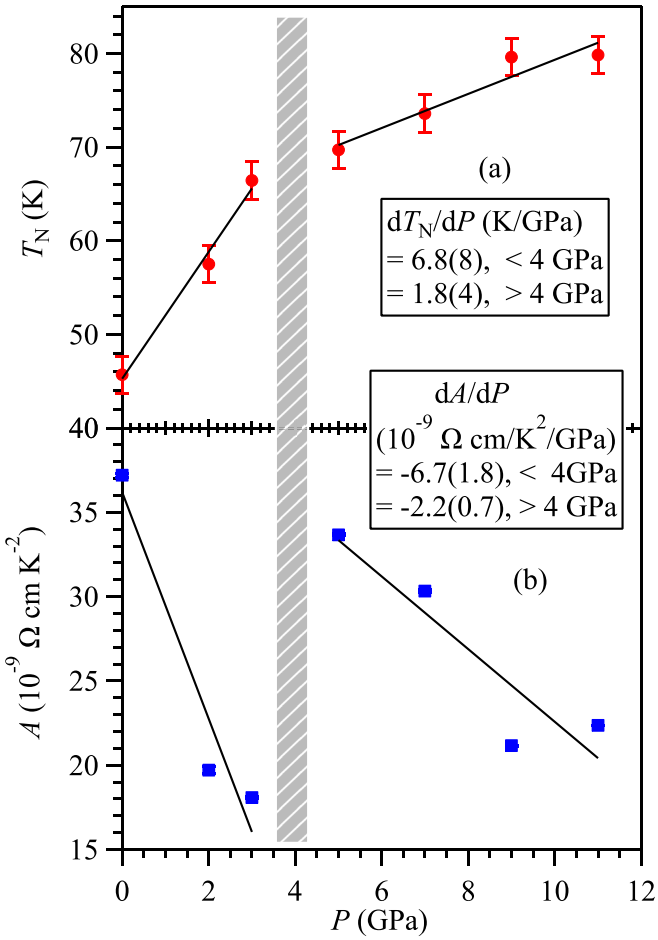

FIG. 3. Pressure dependence of (a) the antiferromagnetic transition temperature T_N and (b) the quadratic-T coefficient A of the Pb_2CoOsO_6 single crystal.

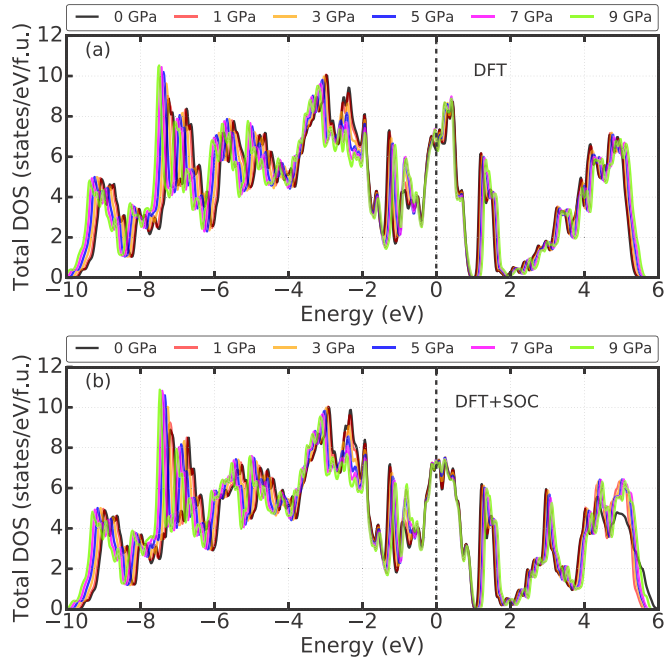

FIG. 4. The total density of states (DOS) of Pb_2CoOsO_6 under 0, 1, 3, 5, 7, and 9 GPa, obtained from (a) spin-polarized DFT calculations and (b) DFT+SOC calculations. Note that in panel (a), the spin up and spin down are identical due to the antiferromagnetic ordering, thus, they are summed in the DOS. The dashed line is the Fermi level.

metallic, and the $\rho(T)$ decreases gradually with increasing pressure, in line with the general expectation that pressure broadens the electronic bandwidth. The resistivity anomaly at T_N is clearly visible in the investigated pressure range and moves to higher temperatures with increasing pressure. This can be seen more clearly from the minimum of $d^2\rho/dT^2$ curves in Fig. 2(b). The determined T_N are plotted in Fig. 3(a) as a function of pressure. The transition temperature is almost doubled and reaches ∼80 K at 11 GPa. Interestingly, it is found that $T_N(P)$ exhibits distinct pressure coefficients, i.e., $T_N(P)$ first increases with pressure in a large slope of +6.8(8) K/GPa for $P < 4$ GPa and, then, in a much reduced slope of +1.8(4) K/GPa for $P > 4$ GPa.

In addition to the discontinuous slope change in $T_N(P)$, a closer inspection of the temperature dependence of $\rho(T)$ curves at low temperatures also evidenced a slope change for $P > 3$ GPa. To quantify this change, we have plotted the low-temperature $\rho(T)$ data in the form of $(\rho - \rho_0)$ versus T^2 in Fig. 2(c), which confirms that the Fermi-liquid behavior remains valid in the whole pressure range. The quadratic-temperature coefficient A, determined from the linear fitting in Fig. 2(c) is shown in Fig. 3(b) as a function of pressure. A nonmonotonic evolution with pressure can be clearly seen at ∼4 GPa. Similarly, $A(P)$ also exhibits a discontinuous jump at ∼4 GPa with distinct pressure coefficients, i.e., dA/dP changes from $-6.7 \pm 1.8 \times 10^{-9}$ Ω cm K^{-2} GPa^{-1} at $P <$ 4 GPa to $-2.2 \pm 0.7 \times 10^{-9}$ Ω cm K^{-2} GPa^{-1} at $P > 4$ GPa. Since the A coefficient is proportional to the effective mass of charge carriers, the distinct values of dA/dP imply that the impact of pressure on the electronic structure is altered significantly at ∼4 GPa.

From these above measurements, we can reach the conclusion that the antiferromagnetic metallic state of Pb_2CoOsO_6 is stabilized by pressure, and it seems to enter a distinct state above 4 GPa as illustrated by the different pressure coefficients of $T_N(P)$ and $A(P)$. Since the polar state blow T_N at ambient pressure is driven by the antiferromagnetic ordering involving both Co and Os sublattices, it is essential to understand how the magnetic state evolves under pressure in Pb_2CoOsO_6 in order to gain some insight on the overall structural properties, in particular, polar distortions. However, direct measurements of long-range magnetic order and magnetic moment (especially Os moment) is difficult, even under ambient pressure. Therefore, we perform first-principles calculations in order to elucidate why a new distinct antiferromagnetic metallic state may emerge in Pb_2CoOsO_6 under pressure and to provide detailed electronic/magnetic/structural properties of pressurized Pb_2CoOsO_6, which are not easily measured in experiment.

First, we calculate the electronic structure of Pb_2CoOsO_6 under pressure. The optimized crystal structure of Pb_2CoOsO_6 at 0 K can be found in Table I in the Appendix. Figure 4 shows the total density of states (DOS) of Pb_2CoOsO_6 under 0, 1, 3, 5, 7, and 9 GPa from DFT

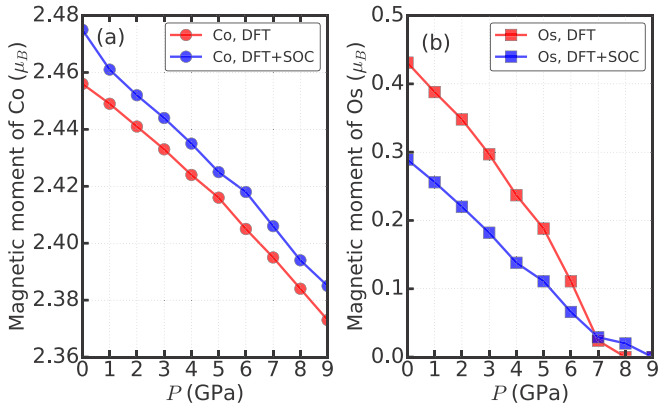

FIG. 5. Magnetic moments of (a) Co and (b) Os in Pb_2CoOsO_6 under 0–9 GPa. The magnetic moments are obtained using DFT and DFT+SOC calculations on the fully optimized crystal structures. The lines are used to guide the eye.

[Fig. 4(a)] and DFT+SOC [Fig. 4(b)] calculations. Because Pb_2CoOsO_6 has an antiferromagnetic ordering, the spin up and spin down are identical in spin-polarized DFT calculations, hence, the two spin-resolved DOS are summed in Fig. 4(a). In DFT+SOC calculations, S_z is no longer a good quantum number, and we show the total DOS. We find from both DFT and DFT+SOC calculations that the effect of pressure on the total DOS is very weak, similar to the previous study on $LiOsO_3$ [18]. Pb_2CoOsO_6 remains metallic under all the pressures in our paper, consistent with the electrical transport measurements. Although standard DFT calculations tend to underestimate band gaps [32], we also find robust metallic properties of Pb_2CoOsO_6 under pressure in our DFT + U ($U_{Co} = U_{Os} = 2$ eV) calculations. By comparing the panels (a) and (b) of Fig. 4, we find that, at a given pressure, the SOC effect on the total DOS is also very weak, especially its effect on the states close to the Fermi level.

Next, we consider the experimentally observed antiferromagnetic ordering in Pb_2CoOsO_6 [19]. Figure 5 shows the evolution of calculated magnetic moments of Co and Os under 0–9 GPa. DFT calculations and DFT+SOC calculations both predict that the magnetic moments of Co and Os decrease monotonically with increasing pressure. The SOC effect tends to decrease the Os magnetic moment but increase the Co magnetic moments. We find that from both DFT and DFT+SOC calculations, there exists a critical pressure $P_c \sim 8$ GPa, above which the Os magnetic moment vanishes, whereas the Co moment only decreases slightly. This has important consequences on the magnetic transition temperature T_N. When the pressure is below the critical pressure, the Néel temperature T_N of Pb_2CoOsO_6 is determined by the two-coupled magnetic sublattices (i.e., Co and Os). However, above the critical pressure, T_N is solely determined by the magnetic sublattice of Co. This may explain the discontinuity of dT_N/dP under pressure in our experiments. We note that the critical pressure estimated from our calculations is larger than the critical pressure observed in experiment. This may result from the approximation of the exchange-correlation functional in our first-principles calculations. Although PBEsol improves the prediction of structural properties of solids, it may overestimate the intrinsic exchange splitting and possibly the magnitude of the Os moment [33,34].

Finally, we study the structural properties of Pb_2CoOsO_6 under pressure. Because each Os moment is surrounded by six Co moments. and these six Co moments form an antiferromagnetic ordering, a finite Os moment causes magnetic frustration in this double perovskite oxide and leads to polar distortions on both Os and Co atoms. We calculate the polar displacements of transition-metal cations (Co and Os) δ along the z direction. δ is defined as $\delta = \frac{1}{4}\sum_{i=1}^{4} d_i$, where $d_i = z_B - z_{O_i}$ and the index i runs over 1–4 because there are four in-plane oxygen atoms in a CoO_6 or OsO_6 octahedron [see Fig. 6(a)]. The polar displacement δ almost linearly decreases with the applied pressure up to 7 GPa as is shown in Fig. 6(b). In the range of 0–7 GPa, the Co polar displacements are substantially stronger approximately ten times) than the Os polar displacements. Our calculations further show that the Co-O and Os-O displacements simultaneously vanish at 8 GPa, coincident with the complete suppression of the Os moment. This is consistent with the picture that the inversion symmetry of Pb_2CoOsO_6 is broken by the magnetic frustration in the antiferromagnetic ordering [19]. With the Os moment vanishing, the magnetic frustration is relieved and,

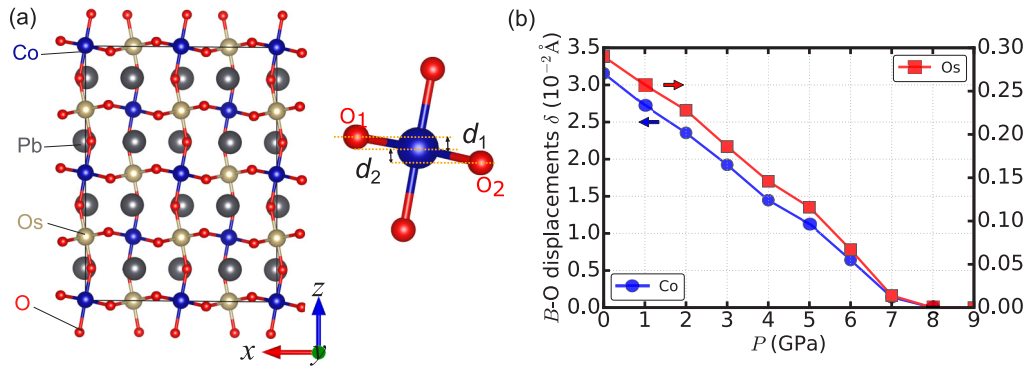

FIG. 6. (a) The optimized crystal structure of Pb_2CoOsO_6 in an 80-atom cell and a metal-oxygen BO_6 octahedron (B = Co or Os). The polar displacement for the B-site metal ion is defined as $\delta = \frac{1}{4}\sum_{i=1}^{4} d_i$ where $d_i = z_B - z_{O_i}$ and the index i runs over 1–4 because there are four in-plane oxygen atoms in a BO_6 octahedron. In panel (a), only d_1 and d_2 are shown for clarity using the black double-headed arrows. (b) The average Co-O and Os-O polar displacements δ in Pb_2CoOsO_6 under 0–9 GPa. The lines in panel (b) are used to guide the eye.

thus, the inversion symmetry is restored. In short, pressure drives Pb_2CoOsO_6 from an antiferromagnetic polar metal (with two types of magnetic ions) to an antiferromagnetic centrosymmetric metal (with only one type of magnetic ion).

IV. CONCLUSION

We perform transport and magnetic measurements and first-principles calculations to study the pressure effect on the recently synthesized type-II polar metal Pb_2CoOsO_6. Experimentally, we monitor the resistivity anomaly at the antiferromagnetic transition T_N under various pressures up to 11 GPa, and found a discontinuous enhancement of $T_N(P)$ from 43 K at ambient pressure to ∼80 K at 11 GPa. The pressure coefficient of $T_N(P)$ decreases significantly from $dT_N/dP = 6.8(8)$ K/GPa for $P < 4$ GPa to 1.8(4) K/GPa for $P > 4$ GPa. Our first-principles calculations suggest that the observed discontinuity of dT_N/dP around ∼4 GPa may be attributed to the disappearance of the Os magnetic moment. Pressure substantially reduces the Os moment, and above a critical value, completely suppresses the Os moment. This relieves the magnetic frustration in the antiferromagnetic ordering of Pb_2CoOsO_6, which, in turn, decreases the Co-O and Os-O polar displacements. Above the critical pressure, both Co and Os atoms move to the centrosymmetric positions (i.e., the center of CoO_6 and OsO_6 octahedra), and the inversion symmetry is restored. This leads to a new antiferromagnetic metallic state in pressurized Pb_2CoOsO_6, distinct from the one under ambient pressure.

ACKNOWLEDGMENT

We thank Dr. L. Hu (Tokyo Institute of Technology) for the valuable discussions. This work was supported by the National Key R&D Program of China (Grant No. 2018YFA0305700), the National Natural Science Foundation of China (Grants No. 11874400, No. 11834016, and No. 11874264), the Beijing Natural Science Foundation (Grant No. Z190008), the Strategic Priority Research Program and Key Research Program of Frontier Sciences of the Chinese Academy of Sciences (Grants No. XDB25000000 and No. QYZDB-SSW-SLH013) as well as the CAS Interdisciplinary Innovation Team. H.C. was supported by the National Natural Science Foundation of China under Project No. 11774236 and NYU University Research Challenge Fund. K.Y. was supported by JSPS KAKENHI Grant No. JP20H05276, and a research grant from Nippon Sheet Glass Foundation for Materials Science and Engineering (Grant No. 40-37). NYU-HPC in New York City, Shanghai, and Abu Dhabi campuses provide computational resources.

TABLE I. The cell parameters of noncentrosymmetric Pb_2CoOsO_6: $a = 5.6984$, $b = 5.6083$, $c = 9.45938$ Å, $\alpha = \gamma = 90.0°$, and $\beta = 126.535°$. The number of the space group of Pb_2CoOsO_6 is 7. Note that we use the setting of standard space-group P_c instead of the nonstandard space-group P_n used in Ref. [19].

Site	Wyckoff Positions	x	y	z
Pb1	2*a*	0.26389	0.25222	0.25229
Pb2	2*a*	0.73935	0.24779	0.75099
Co	2*a*	0.00529	0.75035	0.00388
Os	2*a*	0.49961	0.74996	0.50011
O1	2*a*	0.19200	0.74949	0.25227
O2	2*a*	0.80921	0.75062	0.74717
O3	2*a*	0.29405	0.00817	0.03748
O4	2*a*	0.70126	0.49262	−0.04084
O5	2*a*	0.29952	0.49763	0.03726
O6	2*a*	0.69581	0.00158	−0.04061

APPENDIX: THE DFT OPTIMIZED CRYSTAL STRUCTURE OF Pb_2CoOsO_6 AND THE DISCUSSION OF JAHN-TELLER DISTORTIONS

Table I shows the optimized crystal structure obtained from our DFT calculations under 0 GPa. The DFT-calculated crystal structures of Pb_2CoOsO_6 under pressures up to 9 GPa are available in Ref. [35].

We note that the Jahn-Teller distortions may be associated with the phase transitions in transition-metal oxides under pressures [36], hence, we study the possible Jahn-Teller distortions in CoO_6 and OsO_6 octahedra for the optimized structures under pressures. We follow Ref. [37] and define a Jahn-Teller distortion parameter δ for both CoO_6 and OsO_6 octahedra: $\delta = \frac{l-s}{2(l+s)}$ where l and s are the longer and shorter M-O (M = Os or Co) bond lengths on the MO_4 plane. Using this method, we find that the Jahn-Teller distortion δ for both CoO_6 and OsO_6 octahedra are on the order of 10^{-5} under pressures up to 9 GPa. This indicates that Jahn-Teller distortions in Pb_2CoOsO_6 are very weak both under ambient conditions and under pressures. Therefore, we can conclude that the Jahn-Teller distortion are not correlated to the observed magnetic transitions.

[1] W. Eerenstein, N. Mathur, and J. F. Scott, Nature (London) **442**, 759 (2006).
[2] R. Resta, J. Phys. Condens. Matter **14**, R625 (2002).
[3] P. W. Anderson and E. I. Blount, Phys. Rev. Lett. **14**, 217 (1965).
[4] Y.-W. Fang, H.-C. Ding, W.-Y. Tong, W.-J. Zhu, X. Shen, S.-J. Gong, X.-G. Wan, and C.-G. Duan, Sci. Bull. **60**, 156 (2015).
[5] N. A. Spaldin and R. Ramesh, Nature Mater. **18**, 203 (2019).
[6] S. Dong, H. Xiang, and E. Dagotto, Natl. Sci. Rev. **6**, 629 (2019).
[7] Y. Shi, Y. Guo, X. Wang, A. J. Princep, D. Khalyavin, P. Manuel, Y. Michiue, A. Sato, K. Tsuda, S. Yu, M. Arai, Y. Shirako, M. Akaogi, N. Wang, K. Yamaura, and A. T. Boothroyd, Nature Mater. **12**, 1024 (2013).
[8] H. J. Xiang, Phys. Rev. B **90**, 094108 (2014).
[9] D. Puggioni and J. M. Rondinelli, Nat. Commun. **5**, 1 (2014).

[10] Z. Fei, W. Zhao, T. A. Palomaki, B. Sun, M. K. Miller, Z. Zhao, J. Yan, X. Xu, and D. H. Cobden, Nature (London) **560**, 336 (2018).
[11] Y. Mochizuki, Y. Kumagai, H. Akamatsu, and F. Oba, Phys. Rev. Materials **2**, 125004 (2018).
[12] D. Du, A. Lim, C. Zhang, P. J. Strohbeen, E. H. Shourov, F. Rodolakis, J. L. McChesney, P. Voyles, D. C. Fredrickson, and J. K. Kawasaki, APL Mater. **7**, 121107 (2019).
[13] H. Zhang, W. Huang, J.-W. Mei, and X.-Q. Shi, Phys. Rev. B **99**, 195154 (2019).
[14] J.-J. Gao, S.-Y. Fu, K. Yamaura, J. F. Lin, and J.-S. Zhou, Phys. Rev. B **101**, 220101(R) (2020).
[15] P. A. Volkov and P. Chandra, Phys. Rev. Lett. **124**, 237601 (2020).
[16] J. Lu, G. Chen, W. Luo, J. Íñiguez, L. Bellaiche, and H. Xiang, Phys. Rev. Lett. **122**, 227601 (2019).
[17] Y.-W. Fang and H. Chen, Commun. Mater. **1**, 1 (2020).
[18] E. I. Paredes Aulestia, Y. W. Cheung, Y.-W. Fang, J. He, K. Yamaura, K. T. Lai, S. K. Goh, and H. Chen, Appl. Phys. Lett. **113**, 012902 (2018).
[19] A. J. Princep, H. L. Feng, Y. F. Guo, F. Lang, H. M. Weng, P. Manuel, D. Khalyavin, A. Senyshyn, M. C. Rahn, Y. H. Yuan, Y. Matsushita, S. J. Blundell, K. Yamaura, and A. T. Boothroyd, Phys. Rev. B **102**, 104410 (2020).
[20] J. van den Brink and D. I. Khomskii, J. Phys.: Condens. Matter **20**, 434217 (2008).
[21] G. A. Samara, T. Sakudo, and K. Yoshimitsu, Phys. Rev. Lett. **35**, 1767 (1975).
[22] T. Ishidate, S. Abe, H. Takahashi, and N. Môri, Phys. Rev. Lett. **78**, 2397 (1997).
[23] S. Klotz, J. Chervin, P. Munsch, and G. Le Marchand, J. Phys. D: Appl. Phys. **42**, 075413 (2009).
[24] D. Errandonea, Y. Meng, M. Somayazulu, and D. Häusermann, Physica B: Condens. Matter **355**, 116 (2005).
[25] J.-G. Cheng, K. Matsubayashi, S. Nagasaki, A. Hisada, T. Hirayama, M. Hedo, H. Kagi, and Y. Uwatoko, Rev. Sci. Instrum. **85**, 093907 (2014).
[26] P. E. Blöchl, Phys. Rev. B **50**, 17953 (1994).
[27] G. Kresse and J. Furthmüller, Comput. Mater. Sci. **6**, 15 (1996).
[28] G. Kresse and J. Furthmüller, Phys. Rev. B **54**, 11169 (1996).
[29] J. P. Perdew, A. Ruzsinszky, G. I. Csonka, O. A. Vydrov, G. E. Scuseria, L. A. Constantin, X. Zhou, and K. Burke, Phys. Rev. Lett. **100**, 136406 (2008).
[30] S. L. Dudarev, G. A. Botton, S. Y. Savrasov, C. J. Humphreys, and A. P. Sutton, Phys. Rev. B **57**, 1505 (1998).
[31] R. Morrow, R. Mishra, O. D. Restrepo, M. R. Ball, W. Windl, S. Wurmehl, U. Stockert, B. Büchner, and P. M. Woodward, J. Am. Chem. Soc. **135**, 18824 (2013).
[32] J. Ruiz-Fuertes, S. López-Moreno, J. López-Solano, D. Errandonea, A. Segura, R. Lacomba-Perales, A. Muñoz, S. Radescu, P. Rodríguez-Hernández, M. Gospodinov, L. L. Nagornaya, and C. Y. Tu, Phys. Rev. B **86**, 125202 (2012).
[33] H. Chen and A. J. Millis, Phys. Rev. B **93**, 205110 (2016).
[34] Y.-W. Fang, R. Yang, and H. Chen, J. Phys.: Condens. Matter **31**, 445803 (2019).
[35] Y.-W. Fang and H. Chen, "Dataset for coupled magnetic and structural phase transitions in antiferromagnetic polar metal Pb_2CoOsO_6 under pressure" [https://doi.org/10.5281/zenodo.4033535].
[36] J. Ruiz-Fuertes, A. Segura, F. Rodríguez, D. Errandonea, and M. N. Sanz-Ortiz, Phys. Rev. Lett. **108**, 166402 (2012).
[37] E. Pavarini, E. Koch, and A. I. Lichtenstein, Phys. Rev. Lett. **101**, 266405 (2008).